

## MICROSTRUCTURE EVOLUTION AND PHASE TRANSFORMATION IN QUATERNARY CO-9Al-10W-4Mo ALLOY DURING HEAT TREATMENT

Lihui Zhang<sup>1</sup>, Zhijun Sun<sup>1</sup>, Yuan Li<sup>1</sup>, Yunsong Zhao<sup>1</sup>, Hao Zhao<sup>2</sup>

<sup>1</sup>Beijing Institute of Aeronautical Materials, P.R. China;

<sup>2</sup>China Electronic Product Reliability and Environmental Testing Research Institute, P.R. China  
lihui.zhang@biam.ac.cn, zhijun.sun@biam.ac.cn, yunsong.zhao@biam.ac.cn, zhaohao1@ceprei.com

**Abstract.** Alloy Co-9Al-10W-4Mo was investigated on the microstructure and phase transformation, the following results were obtained. Eutectic Crystal containing the  $\mu$  phase and B<sub>2</sub> phase appeared as cast alloy, and solid solution treatment at 1300 °C for 8h homogenized the structure to form the  $\mu$  phase for supersaturation of W. Following aging at 900 °C for 50 h induces the rod-like DO<sub>19</sub> phase precipitation in the  $\gamma/\gamma'$  matrix structure. DO<sub>19</sub> phase appeared between  $\mu/\gamma$  interface after aging at 900 °C for 300 h and 600 h and promoted more transformation from the  $\mu$  phase to DO<sub>19</sub> phase. Diffusion of W/Mo between the  $\mu$  phase and matrix after long term aging is the main factor that induces phase transformation. Addition of Mo to Co-9Al-10W alloy prompts precipitation of the  $\mu$  phase, and Mo was a W-like element. Formation of the DO<sub>19</sub> phase in the interface decreases the interface energy induced by misfit between  $\mu/\gamma$  crystallographic parameter.

**Keywords:** Co-base superalloys, precipitation, phase transformation, microstructure.

### Introduction

The  $\gamma/\gamma'$  two-phase Co-Al-W and Co-Al-W based superalloys has received considerable attention recently since the stable ternary Co<sub>3</sub>(Al, W) intermetallic compound with L1<sub>2</sub> structure was discovered by Sato et al [1-3]. Having the same microstructure in morphology as  $\gamma/\gamma'$  two-phase Ni-base superalloys, Co-Al-W and its based superalloys have cuboidal  $\gamma'$  precipitations align regularly in continuous matrix phases. This discovery provides a potential pathway for load-bearing Co-base superalloys, and offers new possibilities for applications in severe environments, such as in the industrial combined-cycle power generation system that utilizes gasified coal rather than natural gas.

Except for  $\gamma$  and  $\gamma'$  phases, phases such as DO<sub>19</sub>,  $\mu$  or B<sub>2</sub> phases which have composition near to Co<sub>3</sub>W, Co<sub>7</sub>W<sub>6</sub> and CoAl respectively are expected to precipitate in these alloys during long-term heat treatment [4; 5]. Precipitations of  $\mu$ (Co<sub>7</sub>W<sub>6</sub>) and DO<sub>19</sub> (Co<sub>3</sub>W) phases consume large amount of the refractory element W which strengthens the  $\gamma'$  matrix [6; 7]. In other aspect,  $\mu$  phase belongs to Topologically Closed-packed phase (TCP), belongs to intermetallic which is brittle and prohibits its usage [8]. Therefore, precipitation of  $\mu$  phase and other minor phases during long-term exposure is crucial for studying the formation mechanism and explaining the mechanical properties.

Our attention focused on the behavior of the micro structural changes during heat treatment.

### Experimental Procedure

The nominal composition of the alloys investigated was Co-12Al-10W-4Mo. Alloys were melted as 20 g button ingots using a non-consumable tungsten electrode from starting materials of 99.9 wt% Co, 99.9 wt% Al and 99.9 wt% W. Each button was turned over and remelted 6 times to give a homogeneous specimen. These alloys were homogenized at 1300 °C for 168 h, and then aged at 900 °C for 50 h, 300 h.

The microstructure was examined by scanning electron microscopy (SEM) using ZEISS SUPRA55. Morphology and phase composition were analyzed by JEOL-2010 transmission electron microscopy (TEM) equipped with energy dispersive spectrometers (EDS). Selected area electron diffraction (SAED) was used to identify the kind of phase and their crystallographic relation between the minor phases and bases.

The heat treatment test of large-size samples is carried out in a tubular furnace under air conditions. The alloys in this study use the following two heat treatment methods (if not specifically mentioned): (1) solution treatment: annealing at 1300 °C, cooling for 4 hours, followed by water quenching; (2) aging treatment: 50h, 800 h, 1000 h, 1500 h and 2000 h after 900 °C annealing °C solution treatment and subsequent water quenching treatment. The cast and heat treated standard metallographic samples were prepared with 1% HF, 33% CH<sub>3</sub>COOH, 33% HNO<sub>3</sub> and 33% H<sub>2</sub>O corrosive agents for microstructure inspection. Scanning electron microscopy (SEM) was used to observe the alloy samples in secondary

electron (SE) and backscattered electron (BSE) imaging modes. By observing the cast and heat treated alloys, additional phases besides the  $\gamma$ - and  $\gamma'$ -phases are found. In order to obtain this additional phase, electrolytic extraction experiments were carried out. The structure of this phase was analyzed by X-ray diffraction and the morphology was observed by a scanning electron microscope. In the JEOL 2010 electron microscope with an accelerating voltage of 200 kV, a transmission electron microscope (TEM) is also used for phase recognition. Transmission electron microscope samples were prepared by double jet electropolishing at  $-40\text{ }^{\circ}\text{C}$  and 20V in the solution of 10% perchloric acid, 9% distilled water, 13% butyl cellulose solvent and 68% methanol. Atomic model of  $\mu$  phases was made by Crystal Maker software.

## Results

**Microstructure of As-cast Alloys.** The microstructure of as-cast alloy is shown in Fig. a. It can be seen that the microstructure of the alloy consists of  $\gamma$  matrix and eutectic in the interdendritic regions. Fig. 1(b) is the high magnification BSE image of Fig. 1(a), showing that there are two different phases in the interdendritic region: grey contrast phase and bright contrast phase. The EDS results of the two phases show that the grey phase is consistent with the matrix phase, and the bright mainly phase enriching W and Mo. Referring to the XRD results and the previous reports[1; 9], it is speculated that the matrix and the grey phase were the fcc  $\gamma$  phase, and the bright phase was the  $\text{Co}_7\text{W}_6$  based  $\mu$  phase. No additional phase was discovered in the as-cast alloy.

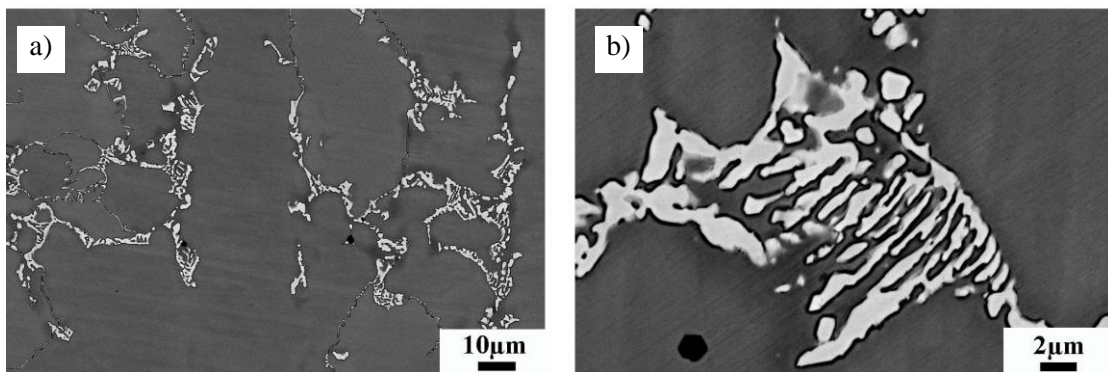


Fig. 1. BSE image of as-cast 9Al-10W-4Mo alloy: a – general microstructure; b – local magnified image in eutectic region

Microstructure of the alloy after solid solution at  $1300\text{ }^{\circ}\text{C}$ . The microstructure of alloy after solid solution is shown in Fig. 2, indicating that the eutectic Co-rich phases resolved completely after solid solution at  $1300\text{ }^{\circ}\text{C}$ . Some rod shaped particles with size of  $2\text{-}5\text{ }\mu\text{m}$  long, and some disc shaped particles with  $2\text{-}5\text{ }\mu\text{m}$  diameter precipitated in the  $\gamma$  matrix. Our former XRD results indicated them to be the  $\mu$  phase[10], and this result indicates that Mo addition of 4% can promote the formation of the  $\mu$  phase.

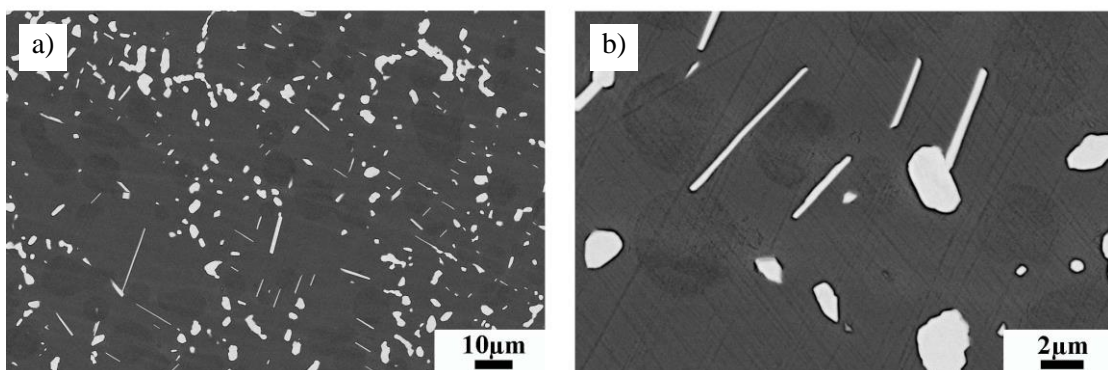


Fig. 2. BSE image of 9Al-10W-4Mo alloy after solid solution under  $1300\text{ }^{\circ}\text{C}$  for 8 h: a) – general microstructure; b) – local magnified image (in the grain)

Microstructure of alloy after aging for different times at  $900\text{ }^{\circ}\text{C}$ . Figure 3 (a)-(d) shows the microstructure of the alloy after aging under  $900\text{ }^{\circ}\text{C}/50\text{ h}$ . With the aging at  $900\text{ }^{\circ}\text{C}$  for 50 h, the amount

of precipitated  $\mu$  phase did not change, while spherical  $\gamma'$  phase precipitated in the matrix as shown in Fig. 3 (b). However, from Fig. 3 (b), we can find grey needle-like phase precipitate. To illuminate morphology of precipitates, the matrix was etched by chemical extraction as shown in Fig. 3 (c). We can find that the  $\mu$  phase has spherical and plate-like morphology which corresponds to the bright contrast phase in the BSE image.

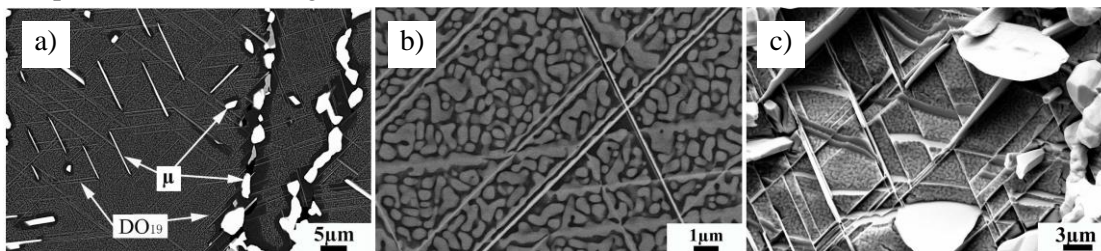


Fig. 3. Images of 9Al-10W-4Mo alloy after aging at 900 °C for 50 h: a – BSE image in general microstructure; b – local magnified image in matrix; c – SEM image in regions containing precipitates after chemical extraction of matrix

TEM analysis of the precipitate shows that in most cases the  $\mu$  phase exists as balls while needle-like precipitates are  $\text{DO}_{19}$  phases. Fig. 4 represents TEM image containing the  $\mu$  phase and  $\text{DO}_{19}$  phase. From elongated diffraction spots in EDP, Fig. 4(b) and 4 (c), we can infer that there exist many planar defects in the  $\mu$  phase, and the needle-like  $\text{DO}_{19}$  phase in this region has a comparatively perfect structure.

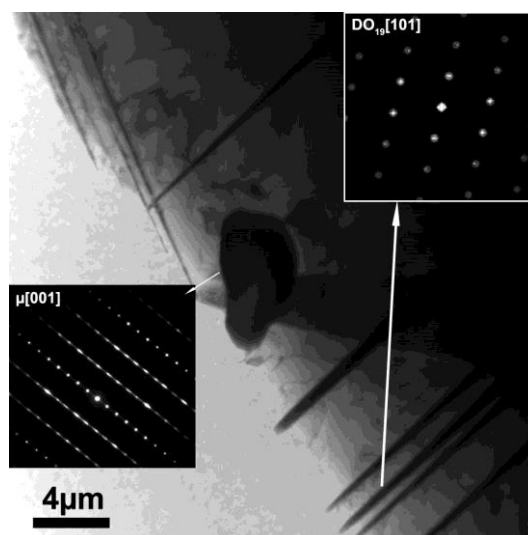


Fig. 4. TEM micrographs and diffraction patterns associated with precipitates

After prolonged aging (900 °C for 300h), the BSE analysis shows no significant increase of bright-contrast precipitates as shown in Fig. 5(a), except a little coarse of them. From the enlarged image in Fig. 5(b), we can find that maze-like  $\gamma'$  appears instead of spherical  $\gamma'$  in alloys aged for 50 h. At the same time, the needle-like  $\text{DO}_{19}$  increases. In some regions, the  $\mu$  phase (bright-contrast) can be found coexisting with some grey-contrast phases which has the same contrast with the needle-like  $\text{DO}_{19}$  phase. EDS analyses indicate that this phase fits for the  $\text{DO}_{19}$  phase in content. Fig. 5(c) and 5(d) show two kinds of coexisting of the  $\mu$  phase and  $\text{DO}_{19}$  phase: in Fig. 5(c), a block-like  $\text{DO}_{19}$  phase embraced the spherical  $\mu$  phase, however, the needle-like  $\text{DO}_{19}$  phase cutting across the block-like  $\mu$  phase is shown in Fig. 5(d).

Figure 6 provides a schematic illustration of the microstructural changes occurring during heat treatment. Three kinds of precipitation ways can be summarized in this illustration. At the top of the illustration, precipitation of the needle-like  $\text{DO}_{19}$  phase is shown. After solid solution, single  $\gamma$  phase is the main except for the  $\mu$  phase; then heat treatment at 900 °C for 50 h induces spherical  $\gamma'$  phase and needle-like  $\text{DO}_{19}$  precipitate; long term aging at 900 °C for 300 h makes spherical  $\gamma'$  transferred to a maze-like cubic with an increase of the  $\text{DO}_{19}$  phase.



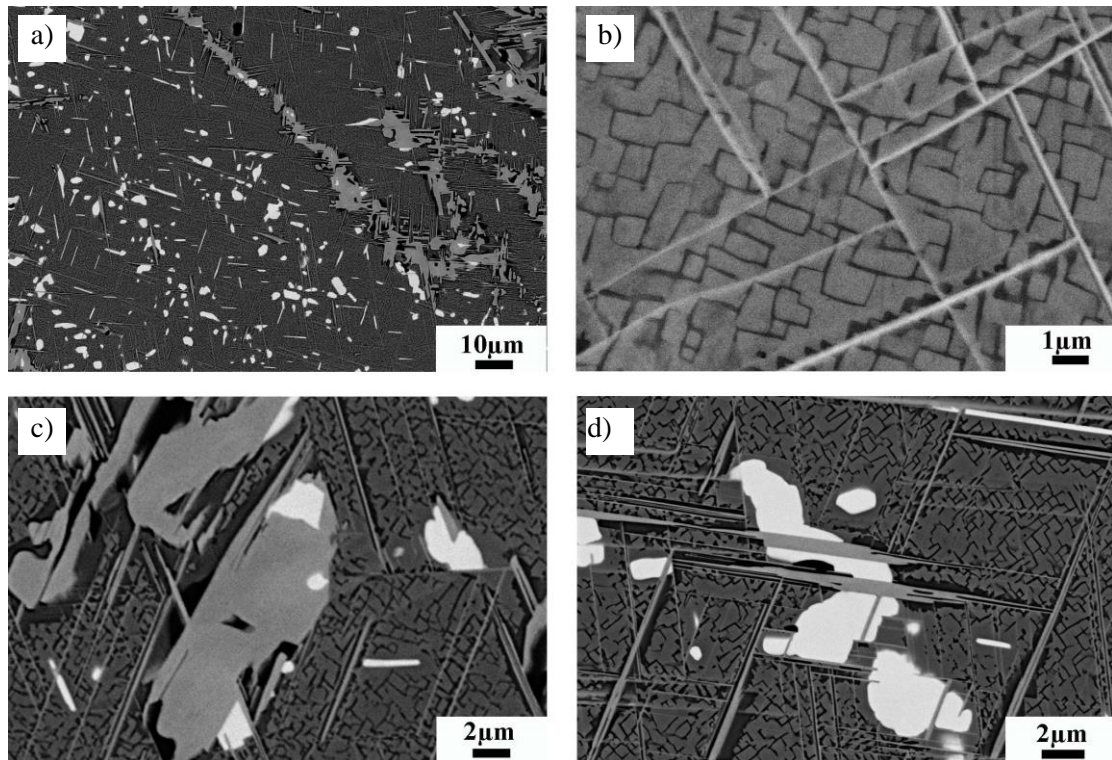


Fig. 5. BSE images of 9Al-10W-4Mo alloy after aging at 900 °C for 300 h:

a – in general microstructure; b – local magnified image in matrix;  
c – local magnified image in precipitation region; d – local magnified image in precipitate region

The other two kinds of precipitation ways are connected with transformation of the  $\mu$  phase and matrix as shown in the middle and bottom of the illustration. After solid solution, the block  $\mu$  phase precipitates in the base; then after aging at 900 for long time for 300 h, the  $DO_{19}$  phase appears in the border of the  $\mu$  phase (middle of the illustration), or as needles cutting through the  $\mu$  phase (bottom of the illustration).

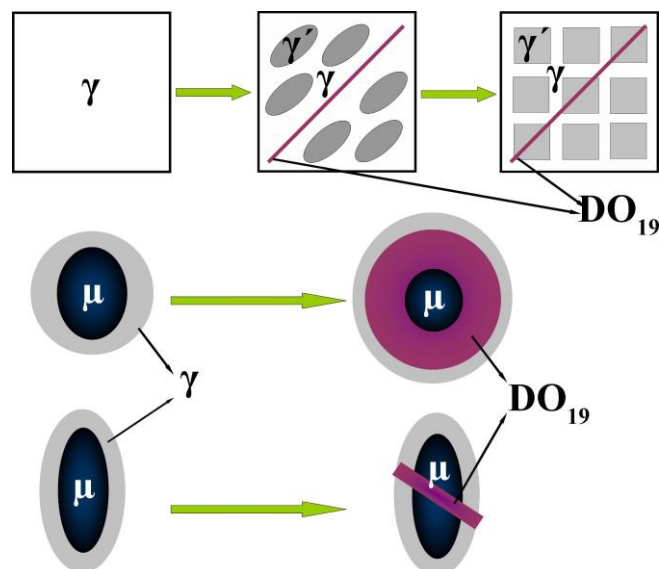


Fig. 6. Schematic illustration of Co-9Al-10W-4Mo alloy after heat treatment

### Discussion

Microstructure affection of Mo addition to Co-9Al-10W. In advanced commercial Ni-base or Co-base superalloys, refractory elements as Mo, Ta, W and Re used to enhance high-temperature strength,

tend to precipitate as TCP or other intermetallic phases during heat treatment. Mo was one of the most important refractory elements and its addition can effectively strengthen Co-Al-W-base superalloy [1]. From bright-contrast precipitates containing Mo/W shown in Fig. 2 and Fig. 4, we can conclude that Mo was a W-equal element. The addition to tungsten saturation alloy (Co-9Al-10W) must induce W/Mo supersaturation in the matrix to form  $\text{Co}_7\text{W}_6/\text{Co}_7\text{Mo}_6$  phases.

Variation of content in the precipitates during precipitation. Precipitates of the  $\mu$  phase after solid solution contain comparative higher content of W and Mo due to supersaturation in the matrix. A heavily content divergence of W/Mo between the  $\mu$  phase and  $\gamma'$  phase will induce diffusion during aging, and the  $\text{DO}_{19}$  phase containing W/Mo between the  $\mu$  phase and  $\gamma'$  phase appears after long time aging for 300 h as shown in the bottom of Fig. 6.

Part of W/Mo that dissolved at 1300 °C after solid solution in the  $\gamma'$  phase will become supersaturated at 900 °C to form  $\text{Co}_3\text{W/Mo}(\text{DO}_{19})$  phase as shown at the top of Fig. 6.  $\text{Co}_3\text{W}(\text{DO}_{19})$  phase has a composition between  $\text{Co}_7\text{W}_6(\mu)$  and  $\text{Co}_3\text{Al}(\gamma/\gamma')$ , and its appearance in a rate weakens their difference during aging to homogenize the alloy.  $\text{DO}_{19}$  phase precipitate more and more with aging time lengthened to form a balanced state. At the same time, with the release of W/Mo from the  $\gamma'$  phase to  $\text{DO}_{19}$  phase and misfit increasing, morphology of the  $\gamma'$  phase transferred from spherical to maze-like square as shown in Fig 5.

Structural relationship connected with phase transformation. In Co-Al-W-Mo alloys, phase transformation from the  $\mu$  phase to  $\text{DO}_{19}$  phase during aging can be attributed to structural similarity among the  $\mu$  phase,  $\text{DO}_{19}$  phase and  $\gamma$  phase on special plane. When the  $\mu$  phase nucleates due to supersaturation of W, they precipitate preferentially on closed-packed planes to form semi coherent interface to decrease the interface energy caused by misfit of the phase and matrix. The orientation relationship of the  $\mu$  phase and matrix in Mo-containing Ni-base superalloys was  $[111]_{\gamma}/[001]_{\mu}[11]$ , and the energy between them is still high in respect of their semi coherent interface. It is known that  $d_{\gamma 111} = 5.85 \text{ \AA}$ , where  $d_{001} = 4.7 \text{ \AA}$ , the large difference of them promotes to form transition phases on the interface during aging to eliminate the interface energy.  $\text{DO}_{19}$  phase has  $d_{001} = 5.12 \text{ \AA}$ , which has a parameter comparative near to base than the  $\mu$  phase has. Appearance of the  $\text{DO}_{19}$  phase,  $\mu$  phase and matrix is necessary to eliminate the energy caused by misfit in  $\mu/\gamma$  interface. In binary Co-W phase diagram in 900 °C,  $\text{Co}_3\text{W}$  is a stable phase, so phase transformation in our alloy from the  $\mu$  phase to  $\text{DO}_{19}$  phase is inevitable after long term aging, and it can be predicted that the  $\text{DO}_{19}$  phase will displace all of the  $\mu$  phase at elevated temperature after long term aging [11; 12].

## Conclusions

Alloy Co-9Al-10W-4Mo was investigated on the microstructure and phase transformation, the following results were obtained.

1. Eutectic Crystal containing  $\mu$  phase and B2 phase appeared as cast alloy, and solid solution treatment at 1300 °C for 8h homogenizes the structure to form the  $\mu$  phase for supersaturation of W. Following aging at 900 °C for 50 h induces the rod-like  $\text{DO}_{19}$  phase precipitate in the  $\gamma/\gamma'$  matrix structure.
2.  $\text{DO}_{19}$  phase appearing between  $\mu/\gamma$  interface after aging at 900 °C for 300 h and 600 h promotes more transformation from the  $\mu$  phase to  $\text{DO}_{19}$  phase.
3. Diffusion of W/Mo between the  $\mu$  phase and matrix after long term aging is the main factor that induces phase transformation.
4. Addition of Mo to Co-9Al-10W alloy prompts precipitation of the  $\mu$  phase, and Mo was a W-like element.
5. Formation of the  $\text{DO}_{19}$  phase in the interface decreases the interface energy induced by misfit between  $\mu/\gamma$  crystallographic parameter.

## Acknowledgements

This work was supported by the Natural Science Foundation of China (Nos. 52001297, 91860202).

## References

- [1] Sato J, Omori T, Oikawa K, et al. Cobalt-base high-temperature alloys. *Science*: 312(5770), 2006, pp. 90-91.
- [2] Chinen H, Sato J, Omori T, et al. New ternary compound  $\text{Co}_3(\text{Ge,W})$  with L12 structure. *Scripta Materialia*: 56(2), 2007, pp. 141-143.
- [3] Shinagawa K, Omori T, Sato J, et al. Phase Equilibria and Microstructure on  $\gamma'$  Phase in Co-Ni-Al-W System. *Materials Transactions*: 49(6), 2008, pp. 1474-1479.
- [4] 李相辉, 甘斌, 冯强, et al. Co-Al-W 三元合金热处理组织 (Heat Treatment Microstructure of Ternary Alloys). *北京科技大学学报*: 30(12), 2008, pp. 1369-1373. (In Chinese)
- [5] 陈艳辉, 龙海波, 毛圣成, et al. 高 Al 新型 Co-Al-W 基高温合金热处理过程中的微观组织演变. (Microstructure evolution of base superalloy during heat treatment) *金属热处理*: 41(7), 2016, 7. (In Chinese)
- [6] Carvalho PA, Haarsma HSD, Kooi BJ, et al. HRTEM study of  $\text{Co}_7\text{W}_6$  and its typical defect structure. *Acta Materialia*: 48(10), 2000, pp. 2703-2712.
- [7] Carvalho PA, Haarsma HSD, Kooi BJ, et al. HRTEM study of  $\text{Co}_{7\text{ sub }7} \text{W}_{6\text{ sub }6}$  and its typical defect structure. *Acta Materialia*: 48(10), 2000, p.
- [8] Tin TMPS. Nickel-Based Superalloys for Advanced Turbine Engines: Chemistry, Microstructure, and Properties. *PROPULSION AND POWER* March-April: Vol. 22, 2006, No. 2.
- [9] Miura S, Ohkubo K, Mohri T. Mechanical properties of Co-based L12 intermetallic compound  $\text{Co}_3(\text{Al,W})$ . *Materials Transactions*: 48(9), 2007, pp. 2403-2408.
- [10] Fei Xue ZL, Yanhui Chen, Qiang Feng. Mo Effect on the Microstructure in Co-Al-W-based Superalloys. The 7th Pacific Rim International Conference on Advanced Materials and Processing (PRICM 7) 2010.
- [11] Yang JX, Zheng Q, Sun XF, et al. Formation of m phase during thermal exposure and its effect on the properties of K465 superalloy. *Scripta Mater*: 55(4), 2006, pp. 331-334.
- [12] Yang J, Zheng Q, Sun X, et al. Morphological evolution of MC carbide in K465 superalloy. *Journal of Materials Science*: 41(19), 2006, pp. 6476-6478.